Microchimica Acta (2019) 186: 348
https://doi.org/10.1007/s00604-019-3478-6

ORIGINAL PAPER

Fluorometric and colorimetric dual-readout alkaline phosphatase activity assay based on enzymatically induced formation of colored Au@Ag nanoparticles and an inner filter effect

Chuanxia Chen[1] · Guanglu Zhang[2] · Pengjuan Ni[1] · Yuanyuan Jiang[1] · Yizhong Lu[1] · Zhengliang Lu[3]

Received: 22 March 2019 / Accepted: 30 April 2019 / Published online: 11 May 2019

Abstract

An ultrasensitive fluorometric and colorimetric dual-mode assay is described for the determination of the activity of alkaline phosphatase (ALP). ALP catalyzes the decomposition of 2-phospho-L-ascorbic acid, and the ascorbic acid thus generated reduces silver ions. In the presence of gold nanoparticles, gold-silver nanoparticles (Au@Ag NPs) are formed. This is accompanied by a color change form pink to deep yellow. The Au@Ag NPs reduce the fluorescence of blue fluorescent graphene quantum dots due to spectral overlap. The changes of absorbance (measured at 410 and 520 nm) and fluorescence (measured at excitation/emission wavelengths of 346/415 nm) correlate well with the ALP activity in the 0.01–6 mU·mL^{-1} (absorption) and 0.01–2 mU·mL^{-1} (fluorescence) ranges, and the detection limits are 9 and 5 μU·mL^{-1} individually.

Keywords Ascorbic acid · Gold-silver nanoparticles · Graphene quantum dots · Fluorescence · Spectral overlap · Quencher · Pyrolysis

Introduction

Multi-signal assays for biomolecules have attracted great attention because they offer more than one kind of output modes simultaneously, thus improving accuracy and diversity by integrating the merits of each output [1]. The most widely used multi-signal assays are colorimetric and fluorometric dual-mode assays. They combine the high sensitivity of fluorescent assay and the convenience, low-cost and visualization of colorimetric assay into one assay. The simultaneous changes in optical signals enhance the accuracy and diversity of the assay. Certain organic molecules [2, 3] and fluorescent nanomaterials [4] can serve as double signal indicators in dual-mode assays by participating in both chromogenic and fluorescence reactions. Among them, o-phenylenediamine is a favorite organic molecular indicator. It is oxidized into 2,3-diaminophenazine that exhibits both colorimetric and fluorescence signals in the presence of catalyst [2, 5, 6]. Fluorescence nanomaterials possessed peroxidase-like activity such as BSA-AuNCs also have been explored as double signal indicators [4]. Such kind of dual-mode assays rely on single material, and always involve organic reagent or time-consuming, time-dependent catalytic reaction. As an alternative, dual-mode assay with two distinct materials as individual fluorescent indicator and colorimetric indicator offers more opportunities to improve the assay performance by varying the properties or types of indicators. Gold nanoparticles (Au NPs) and silver nanoparticles (Ag NPs) have proved to be excellent colorimetric probes and nanoquenchers due to their high

Electronic supplementary material The online version of this article (https://doi.org/10.1007/s00604-019-3478-6) contains supplementary material, which is available to authorized users.

✉ Chuanxia Chen
mse_chencx@ujn.edu.cn

✉ Yizhong Lu
mse_luyz@ujn.edu.cn

✉ Zhengliang Lu
zhengliang.lu@yahoo.com

[1] School of Materials Science and Engineering, University of Jinan, Jinan 250022, China

[2] College of Chemistry, Chemical Engineering and Materials Science, Key Laboratory of Molecular and Nano Probes (Ministry of Education), Collaborative Innovation Center of Functionalized Probes for Chemical Imaging in Universities of Shandong, Institute of Molecular and Nano Science, Shandong Normal University, Jinan 250014, China

[3] Key Laboratory of Interfacial Reaction & Sensing Analysis in Universities of Shandong, School of Chemistry and Chemical Engineering, University of Jinan, Jinan 250022, China

extinction coefficient, tunable plasmon adsorption feature and strong quenching ability [7–9]. Many fluorescent materials including organic dyes [7, 10], carbon nanomaterial [8, 9], CdTe QDs [11] can serve as efficient fluorescent reporters in this type of assays. Though many advances in dual-signal assays, one with straightforward even visual readouts and high sensitivity for each readout is still urgently needed.

Metal core/shell nanostructures, especially Au@Ag nanostructures, are excellent colorimetric probes because slight variation on shell can cause obvious spectral and color change. Though colorimetric single-mode assays based on Au@Ag nanostructures have been developed for various targets [12–15], seldom attention is payed to Au@Ag nanostructure-involved dual-mode assays. Herein, we speculate that noble metal core/shell NPs would be superior nanoquenchers compared to pure core noble metal nanoparticles. It is worth further study as a thought-provoking topic in dual-mode optical techniques. To our knowledge, no dual-mode enzyme activity assay based on enzymatically induced formation of Au@Ag NPs has been reported. This promotes us to develop dual-mode enzyme nanoprobes based on colored Au@Ag NPs and fluorescent nanomaterials with good fluorescent characteristics. Due to the outstanding fluorescence properties, high stability, low toxicity and good biocompatibility, graphene quantum dots (GQDs) have fuelled intensive research interest in biosensing. GQD-based dual-mode assays can be easily achieved by incorporating GQDs into inner filter effects (IFE) or fluorescence resonance energy transfer (FRET) systems.

Alkaline phosphatase (ALP) is generally regarded as a significant biomarker for diagnostics. Abnormal level of ALP in serum has close connection to many diseases, such as prostatic cancer, breast cancer, diabetes, bone disease and liver dysfunction [16]. Therefore, determining ALP activity in human serum is very essential for auxiliary diagnosis of ALP-related diseases. Optical analytical techniques featured with rapidity, simplicity and accessible instrument requirement are well-suited for analysis of ALP activity. With the rapid development of nanotechnology, several noble NP-related colorimetric ALP assays have been reported based on the distance-dependent optical properties [16–19]. However, these colorimetric ALP assays usually suffer from inadequate sensitivity. As a substitute, fluorescent ALP assays with improved sensitivity have been developed based on organic probes [20–23], nanoclusters [24], metal-organic framework [25], carbon dots [26] and GQDs [27, 28]. Most of them require the mediation of transition metal ions or specially designed fluorescence substrates, making them instable or complicated. Additionally, single-mode assays are susceptible to interferences from practical samples. Fluorometric and colorimetric dual-mode assays can provide satisfactory simplicity, sensitivity and improved accuracy for ALP detection due to their merits mentioned above.

Inspired by the views mentioned above, we have proposed an ultrasensitive fluorometric and colorimetric dual-mode assay platform for ALP activity via ALP-mediated in-situ formation of Au@Ag NPs in the presence of fluorescent GQDs. 2-phospho-L-ascorbic acid (AAP) is used as the substrate of ALP. Ascorbic acid (AA) generated via ALP-catalyzed hydrolysis of AAP rapidly reduces silver ions. With the assistance of Au NPs, Au@Ag NPs are formed with distinct color change. GQDs with a high quantum yield (67%) are synthesized by a simple one-pot pyrolysis treatment, and the fluorescent spectra overlap well with the absorption spectrum of Au@Ag NPs. As a result, Au@Ag NPs are capable of quenching the fluorescence of GQDs via IFE. On this basis, a dual-mode optical ALP assay is rationally devised. To our knowledge, this is the first report of IFE-based fluorometric and colorimetric dual-mode assay for detection of ALP using in-situ formed Au@Ag NPs as both the colorimetric indicators and the quenchers.

Experimental

Materials and reagents

ALP (EC 3.1.3.1) from bovine intestinal mucosa, AAP, AA, trypsin, bovine serum albumin (BSA), citric acid, cysteine, gold(III) chloride trihydrate ($HAuCl_4 \cdot 3H_2O$) and $AgNO_3$ were obtained from Sigma-Aldrich (St. Louis, MO, http://www.sigmaaldrich.com/china-mainland.html). Lysozyme, pepsin and pancreatin were purchased from Macklin Biochemical Technology Co., Ltd. (Shanghai, China, http://www.macklin.cn/). Tollens reagent stock solution (contains 20 mM $[Ag(NH_3)_2]OH$) [29], Au NPs [30], and GQDs [8] were prepared referred to reported articles.

Apparatus

UV-vis spectra were recorded by UV-8000 spectrophotometer (Metash, China). Fluorescence spectra were acquired with a Shimadzu RF-6000 spectrofluorometer (Shimadzu, Japan). Time-resolved fluorescence decay was performed on an Edinburgh FLSP-920 spectrofluorometer (Edinburgh, UK). Fourier transform infrared (FT-IR) spectra data were obtained with a Thermo Nicolet 380 Fourier transform infrared spectrometer (USA). Transmission electron microscopy (TEM) images were taken on a Tecnai G2 F20 (FEI) transmission electron microscope operated at 200 kV. X-ray photoelectron spectroscopy (XPS) study was carried out using the ESCALAB MK II spectrometer (VG Scientific) with Al Kα radiation as X-ray source. X-ray powder diffraction (XRD) spectrum were measured using Bruker D8 Advance (Bruker AXS, Germany) with a graphite monochromator using Cu Kα

radiation. Zeta potential was measured by Zetasizer Nano ZS90 System (Malvern).

Detection of ascorbic acid

Typically, 40 μL of AuNP solution (14 nM), 30 μL of GQDs, 10 μL of Tollens reagent (20 mM), 370 μL of ultrapure water and 50 μL of ascorbic acid with various concentrations were sequentially added into 500 μL of Tris buffer (2 mM, pH 9.8). After reaction for 5 min at room temperature, the fluorescence emission spectra centered at 415 nm were measured with 346 nm excitation, and the absorption spectra from 300 to 700 nm range were recorded.

Detection of alkaline phosphatase (ALP) activity

A series of 1.5 mL centrifuge tubes containing 500 μL of Tris buffer (2 mM, pH 9.8), 300 μL of ultrapure water and 20 μL of AAP (10 mM) were loaded with 100 μL of ALP with various activities, and then incubated at 37 °C for 60 min. Subsequently, 40 μL of AuNP solution (14 nM), 10 μL of Tollens reagent (20 mM) and 30 μL of GQDs were successively introduced. After reaction at room temperature for 5 min, the fluorescence emission spectra centered at 415 nm were measured with 346 nm excitation, and the absorption spectra from 300 to 700 nm range were recorded.

Detection of ALP activity in real samples

Twelve serum samples from adult volunteers (from the Hospital of the University of Jinan, Jinan, PR China) were ultrafiltered to remove the redundant salt and small biomolecules with a Microcon centrifugal filter device (Ultracel YM-10 membrance, Millipore). Then the samples were diluted 10 times using 2 mM pH 9.8 Tris buffer, and stored at 4 °C for further use. The feasibility of this dual-mode assay was examined following the procedure "Detection of ALP activity" by just adding the diluted human serum instead of the ALP standard solution.

ALP inhibition assay

First, 50 μL of Na_3VO_4 with various concentrations was incubated with 50 μL of 40 mU·mL^{-1} ALP at room temperature for 15 min. Then, a solution containing 500 μL of Tris buffer (2 mM, pH 9.8), 300 μL of ultrapure water and 20 μL of AAP (10 mM) was sequentially added into these Na_3VO_4-treated ALP solutions. After incubation at 37 °C for 60 min, 40 μL of AuNP solution (14 nM), 10 μL of Tollens reagent (20 mM) and 30 μL of GQDs were successively introduced, and allowed to react for 5 min at room temperature. Finally, the fluorescence emission spectra centered at 415 nm were measured with 346 nm excitation, and the absorption spectra from 300 to 700 nm range were recorded..

Results and discussion

Choice of materials

In this IEF-based fluorometric and colorimetric dual-mode assay, GQDs are chosen as fluorophores, and Au@Ag NPs are chosen as absorbers (nanoquenchers) and colorimetric probes due to their special characteristics. Compared to organic dyes and traditional semiconductor quantum dots, GQDs are superior in excellent stability, low cytotoxicity, high resistance to photobleaching and preferable biocompatibility. The excellent properties of GQDs make them promising signal fragments of dual-mode assays for biomolecules. Au@Ag NPs have extremely large extinction coefficient benefitting from the surface plasmon absorption. Additionally, the absorption of Au@Ag NPs is extremely sensitive to core-to-shell ratio, interparticle distance, and environment, which leads to apparent color change. It means that Au@Ag NPs can be ideal colorimetric probes to enable the colorimetric even visual analysis, and ideal absorbers to modulate the fluorescence of fluorophore in dual-mode assays.

Characterization of Au NPs and GQDs

The optical properties of Au NPs and GQDs are investigated by UV-vis absorption spectra and fluorescence spectra. As shown in Fig. 1a, Au NPs display a prominent SPR absorption at around 520 nm. For GQDs, a typical absorption peaks at 346 nm with a small band at 240 nm are observed (Fig. 1a). The $\pi \rightarrow \pi^*$ transition of C=C centered at 240 nm leads to no observable fluorescence. Whereas, the peak at ca. 346 nm, consistent with band-gap transition, results in strong blue fluorescence emission [31]. The introduction of cysteine in synthetic process uniforms the surface states and efficiently increases the QY of GQDs through doping them with heteroatoms [8]. The GQDs exhibit a high QY of 67.0% with quinine sulfate as the standard (Table S1) and an excitation-independent emission within the excitation wavelength range of 280–400 nm (Fig. 1b). The maximum excitation and emission are located at 346 and 415 nm (Fig. 1a). Fluorescence decay of GQDs can be fitted by a single exponential function with a lifetime of 10.15 ns (Fig. 1c). No discernible variations in appearance and fluorescence intensity are observed for GQDs even after being kept in room temperature for 6 months (Fig. S1), indicating a high stability. Additionally, fluorescence intensity of GQDs changes increasingly with increase of pH values from 1.0 to 6.0, and remains stable in the pH range of 6.0–12.0 (Fig. 1d). The high stability and bright

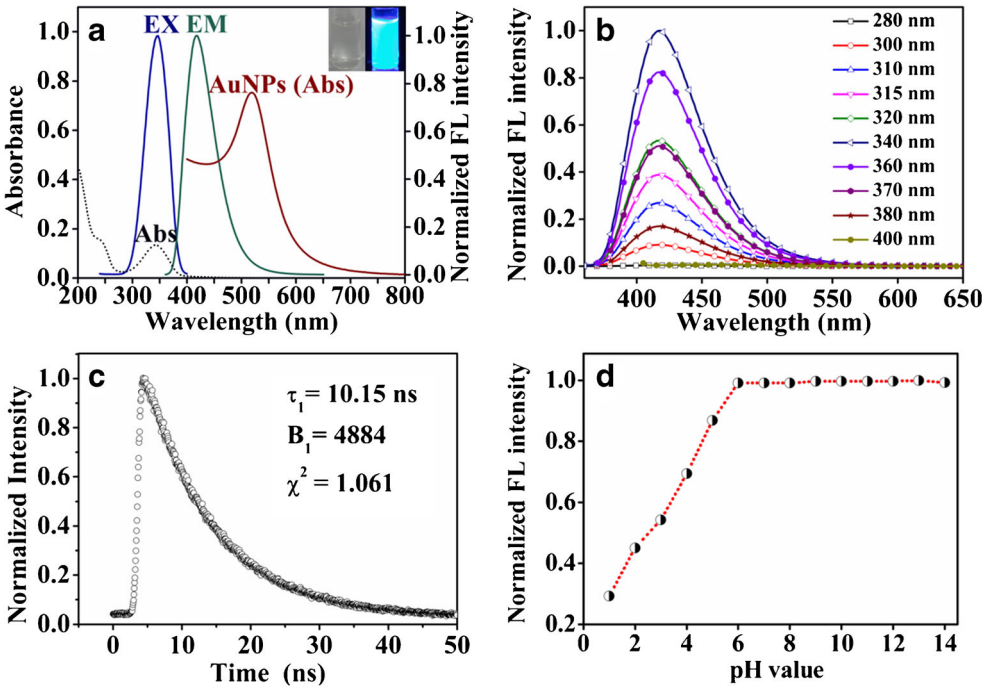

Fig. 1 **a** UV-vis absorption spectra of Au NPs and GQDs, and fluorescence spectra GQDs. Inset: Photographs of GQDs under illumination of daylight and UV (365 nm) light. **b** Fluorescence emission spectra of GQDs with excitation of different wavelength. **c** FL decay spectrum of GQDs. **d** Effect of pH on the fluorescence intensity of GQDs (λex = 346 nm)

fluorescence in neutral and alkaline conditions offer advantages for their future applications in fluorescent detection of biomolecules.

To analyze the structure and composition of GQDs, TEM, XRD, XPS and FT-IR spectra are recorded. Diameters of GQDs are distributed in a narrow range of 1.2–2.6 nm with an average diameter of 1.9 nm (Fig. S2a). The broad (002) peak centers at around 25.5° for GQDs achieved from the XRD pattern confirms GQDs' graphene-like structure (Fig. S2b) [32]. The XPS survey spectrum demonstrated in Fig. S3a shows major peaks at 285, 400, 163 and 532 eV for graphitic C_{1S}, N_{1S}, S_{2P} and O_{1S}. The high-resolution C_{1S} spectrum exhibits three distinct binding energy peaks at 284.5, 286.0 and 288.5 eV (Fig. S3b), demonstrating the presence of C=C/C–C in aromatic rings, C–N (O) and COOH groups. Graphitic structure (sp2 C–C) of GQDs can also be confirmed by the binding energy peak at 284.5 eV. The two peaks at 400.3 and 401.4 eV reveal that both pyridinic type and pyrrolic type N atoms are presented (Fig. S3c). High-resolution spectrum of S_{2P} reveals the presence of C–S–C units (Fig. S3d) [33]. The FT-IR confirms the high occupation of oxygen-rich groups (Fig. S4). The broad band at 3050–3500 cm^{-1} suggests the existence of O–H and N–H. The bands centered at 1708 and 1601 cm^{-1} (vibration bands of C=O) prove the existence of COOH and CONH. In addition, formation of C–N and C–S groups is evidenced by peaks at 1195 cm^{-1}. These results reveal that there are a wealth of –COOH, $–NH_2$ and –OH groups on the surface of GQDs, which endows the GQDs with good hydrophilic properties.

Detection principle of the dual-mode method

Ascorbic acid is an essential micronutrient required for numerous physiological and biological functions in the human body. The most commended property of AA is the splendid reducing capability, based on which it can act as signal transmission medium in several analytical systems of biologically relevant molecules such as bio-enzymes. In this work, a dual-mode optical assay for ALP is rationally designed based on AA induced in-situ formation of Au@Ag NPs by using AAP as the substrate (Fig. 2a). It is well documented that Ag NPs can be produced using AA as reductant [34]. Similarly, AA is able to reduce Tollens reagent (the key component is $[Ag(NH_3)_2]OH$) to generate silver nanoshells coated onto Au NPs, leading to the formation of Au@Ag NPs. The appearance of Ag shell results a new SPR peak at 410 nm, accomplished with a distinct color change from pink to deep yellow (Fig. 2b). The shell thickness is strongly associated with the concentration of AA. What is more, the Au core and Ag shell might exhibit different quenching behavior, which is always be overlooked. We reveal herein that, unlike Au NPs, Au@Ag NPs can readily quench the fluorescence of the GQDs by IFE (Fig. 2a). As control, the sole addition of AA solution or Tollens reagent into Au NPs suspension induce no obvious absorption spectra or color change (Fig. 2b), and emit no fluorescence without GQDs (Fig. 2c). Similarly, the sole addition of AA solution, Tollens reagent or Au NPs to GQDs induce no obvious change in fluorescence spectra (Fig. 2c). These results also confirm that the colorimetric and fluorescent changes are induced by the reduction of Tollens reagent by AA.

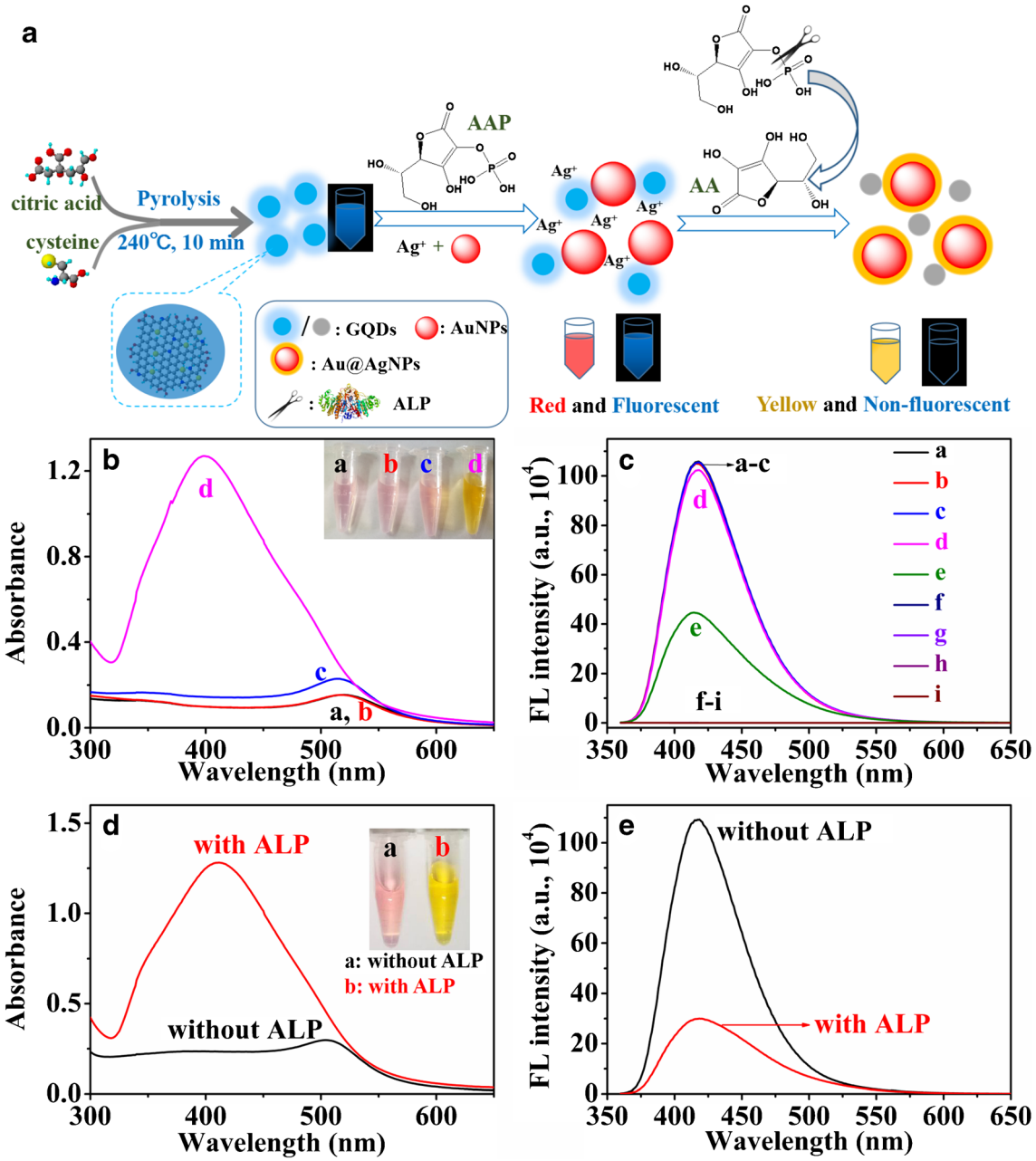

Fig. 2 **a** Detection mechanism based on AA-mediated in-situ formation of Ag@AuNP-GQD ensemble. **b** UV-vis absorption spectra and photographs of Au NPs + GQDs (a), Au NPs + AA + GQDs (b), Au NPs + Tollens reagent + GQDs (c) and Au NPs + Tollens reagent + AA + GQDs (d). **c** Fluorescence emission spectra of GQDs (a), GQDs + Au NPs (b), GQDs + AA (c), GQDs + Tollens reagent (d), GQDs + Au NPs + Tollens reagent + AA (e), Au NPs (g), Au NPs + AA (g), Au NPs + Tollens reagent (h) and Au NPs + Tollens reagent + AA (i). **d** UV-vis absorption spectra and **e** fluorescence emission spectra in the absence (a, black line) and presence of ALP (b, red line). AA, 50 μM; AAP, 0.2 mM; Tollens reagent, 0.2 mM; ALP, 2 mU·mL^{-1}; pH 9.8 (1 mM Tris buffer). λex = 346 nm

ALP is capable of hydrolyzing AAP to produce AA due to its ability to catalyze the dephosphorylation process, thereby, with the aid of AAP, assaying of ALP activity can be achieved (Fig. 2a). It is clearly revealed in Fig. 2d and e that new absorption peak at 410 nm appears and the fluorescence declines significantly with the introduction of ALP. Individual ALP or AAP has no effect on the Au NPs + Tollens reagents system (date are not given). These results suggest the possibility of dual-mode detection of ALP.

To demonstrate the quenching mechanism, a series of characterizations are carried out systematically. Firstly, the structure of generated NPs are characterized. TEM images show that dimensional size of original Au NPs increases with the addition of 30 μM AA due to the deposition of Ag shell (Fig.

S5). Most of the generated NPs are spherical and exhibit inhomogenous electronic density with a darker central part and a lighter outer part (Fig. S6), verifying the formation of Au@Ag core-shell structures. Additionally, the possibility of forming alloys can be ruled out by the fact that HNO_3 dissolves the Ag shell alone but barely affects the Au core (Fig. S7). Subsequently, the fluorescence quenching principle is investigated in detail. As shown in Fig. 3a, the absorption spectrum of Au@Ag NPs (410 nm) shows huge overlapping region with both excitation and emission spectra of GQDs (415 nm), indicating that the efficient fluorescence quenching of GQDs may be attributed to IFE or FRET. Notably, IFE does not require the link of the absorber with the fluorophore while in case of FRET, valid interactions such as electrostatic attraction and covalent binding between them are essential to enable a particular distance between the acceptor and the donor. To provide reassuring support for the quenching mechanism, interactions between Au@Ag NPs and GQDs need to be probed into. The zeta potential of Au NPs, Au@Ag NPs and GQDs in Tris buffer (pH 9.8) are measured to be −21.1 eV, −17.7 eV and − 54.3 eV respectively, suggesting the lack of electrostatic interaction between them. In addition, when Au@Ag NPs are removed from the mixture of Au@Ag NPs and GQDs by centrifugation, fluorescence of the supernatant recovers to approximately 95% of the initial intensity of sole GQDs (Fig. 3b). Moreover, there are no significant variations on the fluorescence of sole GQDs and GQD-Au NPs after centrifugation. These results eliminate the possibility of formation of any complex between GQDs and Au@Ag NPs or Au NPs, thus excluding the possible binding between Au@Ag NPs and GQDs. Hence, on the basis of above observation, we can state that IFE is the dominate reason for the fluorescence quenching and eventually accountable for remarkable sensitivity toward target detection. The fluorescence quenching efficiency is also analyzed. With increasing concentration of Au@Ag NPs, the fluorescence of GQDs gradually decreases (Fig. S8a). The Stern-Volmer plot shown in Fig. S8b does not fit a conventional linear Stern-Volmer equation. The upward-curving Stern-Volmer plot indicates both dynamic and static quenching processes occur in this system [35].

Assessment of the dual-mode method for ascorbic acid quantization

Reaction time of generating Au@Ag NPs and concentration of Tris buffer (pH 9.8) are firstly investigated. The reaction is finished within 5 min (Fig. S9). This is much shorter compared to the system using $AgNO_3$ and without Au NPs [5]. It indicates that the introduction of Au NPs and the use of Tollens reagent have effectively shorten the response time. Tris buffer with high concentration has negligible effect on the value of A_{410}/A_{520}, but takes longer time to finish the reaction (Fig. S10). So 1 mM Tris buffer is used in the subsequent experiments. Under the optimal conditions, the SPR peak at 520 nm blue shifts and the SPR band at 410 nm increases progressively with the incremental concentration of AA (Fig. S11a). This is accompanied by a color change from pink to orange and finally yellow (Fig. S11c). The A_{410}/A_{520} ratio correlates well to the concentration of AA over the range of 1–50 μM (inset in Fig. S11a). As designed, the fluorescence intensity at 415 nm decreases gradually (Fig. S11b). The fluorescence quenching efficiency ($1\text{-}F/F_0$, where F_0 and F represent the fluorescence intensity in the absence and presence of AA, respectively) versus AA displays good linearity in the range of 1–40 μM (inset in Fig. S11b). The sensitive quantization of AA lays a foundation for assessing ALP activity using AAP as the substrate.

Assessment of this assay for ALP activity based on ascorbic acid detection

For efficient detection of ALP activity, several experimental conditions have been optimized firstly, and an incubation time of 60 min, 0.2 mM AAP, and 0.2 mM Tollens reagent are finally chosen (Fig. S12). Then, the colorimetric and fluorescence responses of the system toward ALP with various

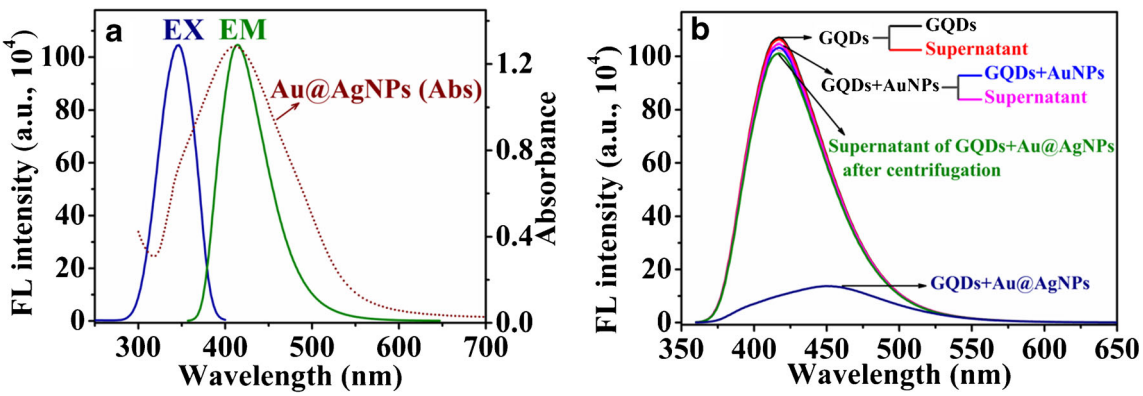

Fig. 3 **a** UV-vis absorption spectrum of Au@Ag NPs and fluorescence spectra of GQDs. **b** Centrifugation of GQDs, GQDs-Au NP mixture, and GQDs-Au@Ag NP mixture

activities are studied and depicted in Fig. 4. With ALP activity increases from 0 to 8.0 mU·mL^{-1}, the SPR band at 410 nm increases gradually with blue shift of the SPR peak at 520 nm (Fig. 4a) due to the incremental concentration of generated AA. Correspondingly, the solution color varies from pink to yellow via orange (Insert in Fig. 4a). When ALP exceeds 0.2 mU·mL^{-1}, an apparent color change can be visually differentiated from the initial one. As manifested in Fig. 4b, the A_{410}/A_{520} ratio correlates well to the ALP activities in the range of 0.01–6.0 mU·mL^{-1} ($R^2 = 0.998$). Additionally, the fluorescence emission spectra centered at 415 nm decrease gradually (Fig. 4c), and there is a good linear relationship between fluorescence quenching efficiency and ALP activities over the range of 0.01–2.0 mU·mL^{-1} ($R^2 = 0.990$, Fig. 4d). On the basis of 3σ/S, detection limits are calculated to be 9 μU·mL^{-1} and 5 μU·mL^{-1} for colorimetric and fluorescent methods, respectively. The sensitivity is superior to most reported methods (Table S2). Besides high sensitivity, intrinsic high specificity of enzyme reaction would confirm an ideal selectivity for ALP detection. Some representative proteins and enzymes, including BSA, lysozyme, pepsin, panceatin, and trypsin (10 μg·mL^{-1}) are performed as control. The results in Fig. S13 persuasively show that none, except ALP, can evoke conspicuous colorimetric and fluorescent signals and disturb the analysis of ALP activity, manifesting a satisfactory selectivity for ALP detection. This outstanding selectivity is ascribed to the high specificity of ALP-catalyzed dephosphorylation of AAP. Other species are unable to hydrolyze AAP and generate reducing agent, and thus cannot reduce Tollens reagent to generate Au@Ag NPs.

Besides, to make a comparison, we also have determined the ALP activity using the same system except excluding Au NPs (Fig. S14). When ALP is introduced, Ag NPs are generated, along with the emergence of SPR peak at around 412 nm. With the increase of ALP activities from 0.2 to 10 mU·mL^{-1}, both absorption spectra and absorbance intensities at 412 nm stepwise increase (Fig. S14a, b). The detection limit is 0.19 mU/mL, which is 2 order of magnitude higher than that of Au NP-involved colorimetric method. The ALP activity can be visually differentiated (0.8 mU·mL^{-1}, Fig. S14e) is also higher than the designed one (0.2 mU·mL^{-1}). In the case of fluorescent detection, the linear range is 0.05–2 mU·mL^{-1} with a detection limit of 0.034 mU·mL^{-1} (Fig. S14c, d), which is inferior to the designed fluorescent method. Obviously, the introduction

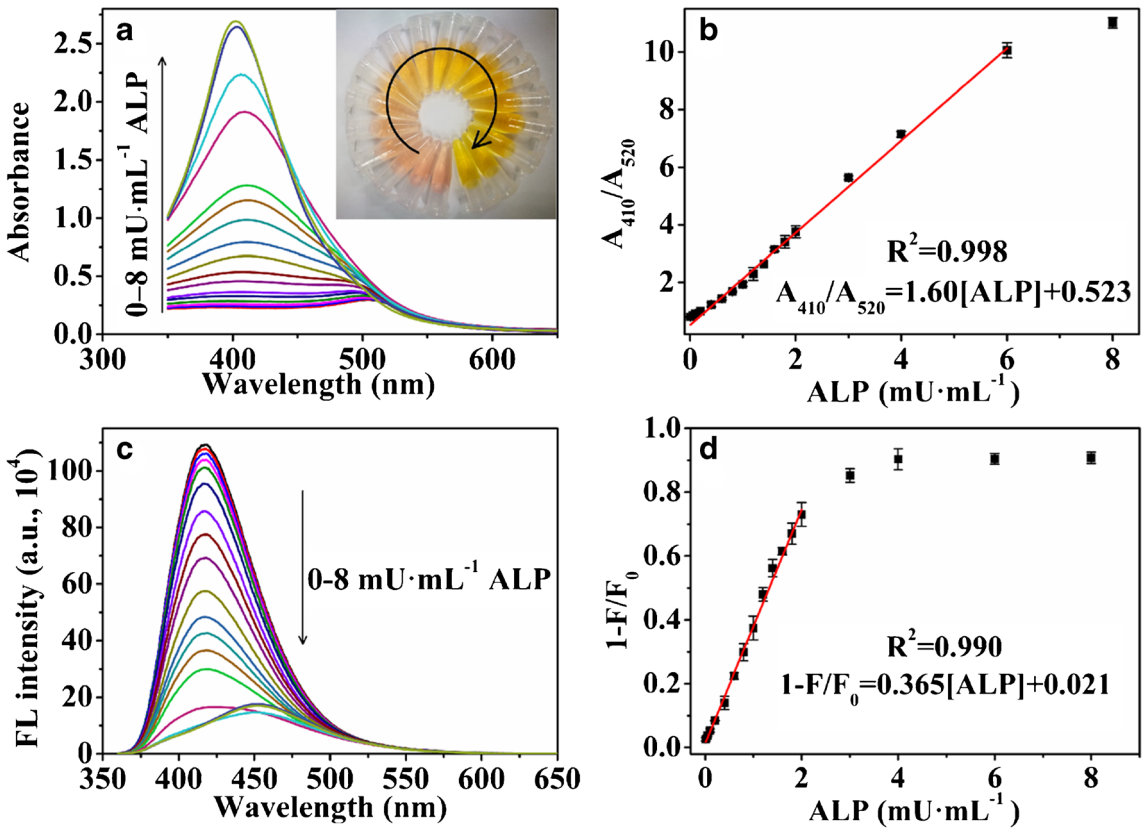

Fig. 4 **a** UV–vis absorption spectra and the corresponding color change, **b** absorbance change (A_{410}/A_{520}), **c** fluorescence emission spectra and **d** fluorescence decrease efficiency of the system in the presence of different concentrations of ALP (0, 0.01, 0.05, 0.1, 0.2, 0.4, 0.6, 0.8, 1, 1.2, 1.4, 1.6, 1.8, 2, 3, 4, 6, 8 mU·mL^{-1}). AAP, 0.2 mM; Tollens reagent, 0.2 mM; pH 9.8 (1 mM Tris buffer). The excitation and emission wavelength are 346 nm and 415 nm. Error bar represents the standard deviation ($n = 3$)

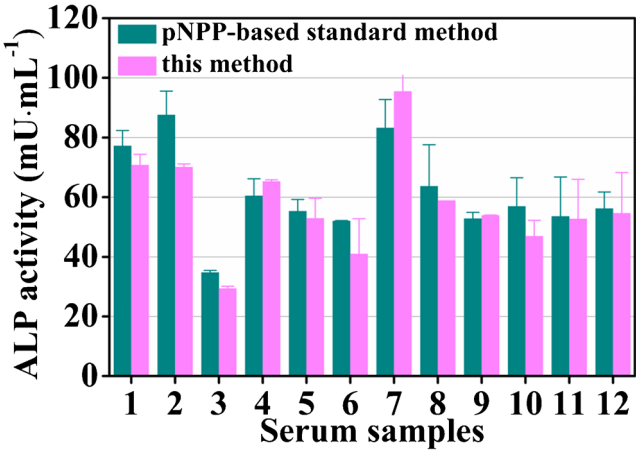

Fig. 5 Detection of ALP in 12 adult volunteer serums by our method and the pNPP-based standard chromogenic method. The excitation and emission wavelength are 346 nm and 415 nm. Error bar represents the standard deviation ($n = 3$)

of Au NPs has remarkably enhanced the sensitivity for both colorimetric and fluorescent detection, which also make the visual identification more easier.

Detection of ALP in human serum samples

As the normal range of ALP in adults is 46–190 mU/mL [18], this assay is sensitive enough for practical detection of ALP level in human body. To ensure the practicability and reliability of this method, twelve serum samples collected from adult volunteers are analyzed and compared with the well-known pNPP-based standard chromogenic method. As depicted in Fig. 5, analytical results obtained from our method are consistent well with those achieved by standard method. These results verify that our technology has potential applications for ALP determination in real samples.

ALP inhibition assay

Investigating the inhibitor of enzyme is of great significance in drug design. Therefore, this method is used to evaluate the enzyme inhibition efficiency. Na_3VO_4, an acknowledged ALP inhibitor, is employed to inhibiting assays. With the addition of Na_3VO_4 into the assay solution, the release of AA (i.e., hydrolysis of AAP) is restricted due to inhibition of ALP activity (2 mU·mL^{-1}). As a result, generation of Au@Ag NPs is depressed, and fluorescence quenching is hindered. Figure 6 manifests that the absorbance decreases progressively and the fluorescence intensity at 415 nm increases progressively with the increase of Na_3VO_4 concentration from 0 to 80 μM. The inhibiting efficiency is expressed by inhibition ratio (I, %), and the relevant equations for colorimetric and fluorescent assays are

$$\mathrm{I}\,(\%) = \frac{A_I - A_0}{A_B - A_0} \times 100\% \quad \text{and} \quad \mathrm{I}\,(\%) = \frac{F_I - F_0}{F_B - F_0} \times 100\%$$

where A_B (F_B) is the initial absorbance (fluorescence intensity) in absence of ALP, A_0 (F_0) stands for the absorbance (fluorescence intensity) in the presence of ALP without inhibitor, and A_I (F_I) is the absorbance (fluorescence intensity) in the presence of ALP with inhibitor. The detection limits are determined to be 12 nM and 5.6 nM for colorimetric and fluorescent detection of Na_3VO_4 based on 3σ/S, indicating the ultrasensitivity. These results indicate that our approach can be used to screen trace ALP inhibitors in drug discovery.

Major limitations of the work

The need for working in the UV (λex = 346 nm) makes the probe prone to interferences by biomatter. Blood, serum, cells, etc. always display strong background UV absorption and fluorescence. The UV light used for fluorescence excitation will be screened off by UV absorbers and this will weaken the

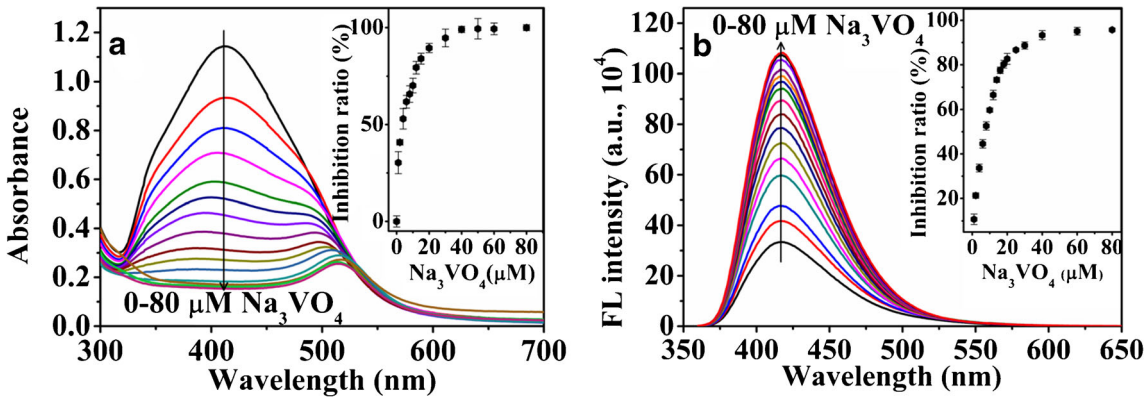

Fig. 6 **a** UV–vis absorption spectra and **b** fluorescence emission spectra of the assay system in the presence of different concentrations of Na_3VO_4 (0, 1, 2, 4, 6, 8, 10, 12, 14, 16, 18, 20, 25, 30, 40, 60, 80 μM). Inserts are their calibration plots. AAP, 0.2 mM; Tollens reagent, 0.2 mM; ALP, 2 mU·mL^{-1}; pH 9.8 (1 mM Tris buffer). λex = 346 nm. Error bar represents the standard deviation ($n = 3$)

signal. The same is true for emitted UV fluorescence which will be screened off.

Conclusions

Based on enzymatically induced formation of Ag@Au NPs in the presence of fluorescent GQDs, an exquisite fluorometric and colorimetric dual-readout optical ALP assay is rationally devised. In this IFE-based assay, Au@Ag NPs behave as colorimetric indicators and nanoquenchers, and GQDs act as fluorescent indicator. The sensitivity is satisfying when compared to other. Although some biomatters can weaken the fluorescent signal, the assay exhibits good performance in evaluating of ALP level in serologic test and for studying the inhibition effect on ALP. Moreover, the method can be expanded to assay other enzymes by changing the AA-involved enzyme substrates.

Acknowledgments This work was supported by the National Natural Science Foundation of China (21705056), the Young Taishan Scholars Program (tsqn201812080) and the Natural Science Foundation of Shandong Province (ZR2018BB057, ZR2017MB022, ZR2018PB009).

Compliance with ethical standards The author(s) declare that they have no competing interests.

References

1. Yin GX, Niu TT, Gan YB, Yu T, Yin P, Chen HM, Zhang YY, Li HT, Yao SZ (2018) A multi-signal fluorescent probe with multiple binding sites for simultaneous sensing of cysteine, homocysteine, and glutathione. Angew Chem Int Ed 57(18):4991–4994. https://doi.org/10.1002/anie.201800485
2. Sun J, Wang B, Zhao X, Li ZJ, Yang XR (2016) Fluorescent and colorimetric dual-readout assay for inorganic pyrophosphatase with Cu^{2+}-triggered oxidation of o-phenylenediamine. Anal Chem 88(2):1355–1361. https://doi.org/10.1021/acs.analchem.5b03848
3. Zhao JH, Bao XF, Wang S, Lu SS, Sun J, Yang XR (2017) In situ fluorogenic and chromogenic reactions for the sensitive dual-readout assay of tyrosinase activity. Anal Chem 89(19):10529–10536. https://doi.org/10.1021/acs.analchem.7b02739
4. Tao Y, Lin YH, Ren JS, Qu XG (2013) A dual fluorometric and colorimetric sensor for dopamine based on BSA-stabilized au nanoclusters. Biosens Bioelectron 42:41–46. https://doi.org/10.1016/j.bios.2012.10.014
5. Liu SG, Han L, Li N, Xiao N, Ju YJ, Li NB, Luo HQ (2018) A fluorescence and colorimetric dual-mode assay of alkaline phosphatase activity via destroying oxidase-like CoOOH nanoflakes. J Mater Chem B 6(18):2843–2850. https://doi.org/10.1039/c7tb03275g
6. Chen CX, Ni PJ, Jiang YY, Zhao ZL, Lu YZ (2018) Dual-mode detection of dopamine based on enhanced fluorescent and colorimetric signals of Fe^{3+}-H_2O_2-o-phenylenediamine system. Chin J Anal Chem 46(8):1231–1237. https://doi.org/10.1016/s1872-2040(18)61103-x
7. Chen CX, Zhao D, Sun J, Yang XR (2016) A dual-mode signaling response of a AuNP-fluorescein based probe for specific detection of thiourea. Analyst 141(8):2581–2587. https://doi.org/10.1039/c6an00165c
8. Chen CX, Zhao D, Hu T, Sun P, Yang XR (2017) Highly fluorescent nitrogen and sulfur co-doped graphene quantum dots for an inner filter effect-based cyanide sensor. Sensors Actuators B Chem 241:779–788. https://doi.org/10.1016/j.snb.2016.11.010
9. Shi Y, Pan Y, Zhang H, Zhang Z, Li MJ, Yi C, Yang M (2014) A dual-mode nanosensor based on carbon quantum dots and gold nanoparticles for discriminative detection of glutathione in human plasma. Biosens Bioelectron 56:39–45. https://doi.org/10.1016/j.bios.2013.12.038
10. Zhao D, Chen CX, Lu LX, Yang F, Yang XR (2015) A dual-mode colorimetric and fluorometric "light on" sensor for thiocyanate based on fluorescent carbon dots and unmodified gold nanoparticles. Analyst 140(24):8157–8164. https://doi.org/10.1039/c5an01926e
11. Gao F, Ye Q, Cui P, Zhang L (2012) Efficient fluorescence energy transfer system between CdTe-doped silica nanoparticles and gold nanoparticles for turn-on fluorescence detection of melamine. J Agric Food Chem 60(18):4550–4558. https://doi.org/10.1021/jf300386y
12. Lin TR, Wu YR, Li ZH, Song ZP, Guo LQ, Fu FF (2016) Visual monitoring of food spoilage based on hydrolysis-induced silver metallization of Au nanorods. Anal Chem 88(22):11022–11027. https://doi.org/10.1021/acs.analchem.6b02870
13. Gao ZQ, Deng KC, Wang X-D, Miro M, Tang DP (2014) High-resolution colorimetric assay for rapid visual readout of phosphatase activity based on gold/silver core/shell nanorod. ACS Appl Mater Interfaces 6(20):18243–18250. https://doi.org/10.1021/am505342r
14. Zeng JB, Fan SG, Zhao CY, Wang QR, Zhou TY, Chen X, Yan ZF, Li YP, Xing W, Wang XD (2014) A colorimetric agarose gel for formaldehyde measurement based on nanotechnology involving tollens reaction. Chem Commun 50(60):8121–8123. https://doi.org/10.1039/c4cc00914b
15. Xian Yu Y, Sun J, Li Y, Tian Y, Wang Z, Jiang X (2013) An ultrasensitive, non-enzymatic glucose assay via gold nanorod-assisted generation of silver nanoparticles. Nanoscale 5(14):6303–6306. https://doi.org/10.1039/c3nr01697h
16. Wei H, Chen CG, Han BY, Wang E (2008) Enzyme colorimetric assay using unmodified silver nanoparticles. Anal Chem 80(18):7051–7055. https://doi.org/10.1021/ac801144t
17. Xianyu YL, Wang Z, Jiang XY (2014) A plasmonic nanosensor for immunoassay via enzyme-triggered click chemistry. ACS Nano 8(12):12741–12747. https://doi.org/10.1021/nn505857g
18. Li CM, Zhen SJ, Wang J, Li YF, Huang CZ (2013) A gold nanoparticles-based colorimetric assay for alkaline phosphatase detection with tunable dynamic range. Biosens Bioelectron 43:366–371. https://doi.org/10.1016/j.bios.2012.12.015
19. Zhao W, Chiuman W, Lam JC, Brook MA, Li Y (2007) Simple and rapid colorimetric enzyme sensing assays using non-crosslinking gold nanoparticle aggregation. Chem Commun (36):3729–3731. https://doi.org/10.1039/b705335e
20. Liu Y, Schanze KS (2008) Conjugated polyelectrolyte-based real-time fluorescence assay for alkaline phosphatase with pyrophosphate as substrate. Anal Chem 80(22):8605–8612. https://doi.org/10.1021/ac801508y
21. Kim TI, Kim H, Choi Y, Kim Y (2011) A fluorescent turn-on probe for the detection of alkaline phosphatase activity in living cells. Chem Commun 47(35):9825–9827. https://doi.org/10.1039/c1cc13819g
22. Li SJ, Li CY, Li YF, Fei J, Wu P, Yang B, Ou-Yang J, Nie SX (2017) Facile and sensitive near-infrared fluorescence probe for the detection of endogenous alkaline phosphatase activity in vivo. Anal Chem 89(12):6854–6860. https://doi.org/10.1021/acs.analchem.7b01351

23. Chen CX, Zhao JH, Lu YZ, Sun J, Yang XR (2018) Fluorescence immunoassay based on the phosphate-triggered fluorescence turn-on detection of alkaline phosphatase. Anal Chem 90(5):3505–3511. https://doi.org/10.1021/acs.analchem.7b05325
24. Wang HB, Li Y, Chen Y, Zhang ZP, Gan T, Liu YM (2018) Determination of the activity of alkaline phosphatase by using nanoclusters composed of flower-like cobalt oxyhydroxide and copper nanoclusters as fluorescent probes. Microchim Acta 185(2):102. https://doi.org/10.1007/s00604-017-2622-4
25. Chen CX, Yuan Q, Ni PJ, Jiang YY, Zhao ZL, Lu YZ (2018) Fluorescence assay for alkaline phosphatase based on ATP hydrolysis-triggered dissociation of cerium coordination polymer nanoparticles. Analyst 143(16):3821–3828. https://doi.org/10.1039/c8an00787j
26. Hu YL, Geng X, Zhang L, Huang ZM, Ge J, Li ZH (2017) Nitrogen-doped carbon dots mediated fluorescent on-off assay for rapid and highly sensitive pyrophosphate and alkaline phosphatase detection. Sci Rep 7:5849. https://doi.org/10.1038/s41598-017-06356-z
27. Chen L, Yang GC, Wu P, Cai CX (2017) Real-time fluorescence assay of alkaline phosphatase in living cells using boron-doped graphene quantum dots as fluorophores. Biosens Bioelectron 96:294–299. https://doi.org/10.1016/j.bios.2017.05.022
28. Liu J, Tang D, Chen Z, Yan X, Zhong Z, Kang L, Yao J (2017) Chemical redox modulated fluorescence of nitrogen-doped graphene quantum dots for probing the activity of alkaline phosphatase. Biosens Bioelectron 94:271–277. https://doi.org/10.1016/j.bios.2017.03.017
29. Dondi R, Su W, Griffith GA, Clark G, Burley GA (2012) Highly size- and shape-controlled synthesis of silver nanoparticles via a templated tollens reaction. Small 8(5):770–776. https://doi.org/10.1002/smll.201101474
30. Grabar KC, Freeman RG, Hommer MB, Natan MJ (1995) Preparation and characterization of Au colloid monolayers. Anal Chem 67(4):735–743. https://doi.org/10.1021/ac00100a008
31. Wang X, Cao L, Yang ST, Lu F, Meziani MJ, Tian L, Sun KW, Bloodgood MA, Sun YP (2010) Bandgap-like strong fluorescence in functionalized carbon nanoparticles. Angew Chem Int Ed 49(31):5310–5314. https://doi.org/10.1002/anie.201000982
32. Liu RL, Wu DQ, Feng XL, Muellen K (2011) Bottom-up fabrication of photoluminescent graphene quantum dots with uniform morphology. J Am Chem Soc 133(39):15221–15223. https://doi.org/10.1021/ja204953k
33. Dong Y, Pang H, Yang HB, Guo C, Shao J, Chi Y, Li CM, Yu T (2013) Carbon-based dots co-doped with nitrogen and sulfur for high quantum yield and excitation-independent emission. Angew Chem Int Ed Engl 52(30):7800–7804. https://doi.org/10.1002/anie.201301114
34. Qin YQ, Ji XH, Jing J, Liu H, Wu HL, Yang WS (2010) Size control over spherical silver nanoparticles by ascorbic acid reduction. Colloids Surf A Physicochem Eng Asp 372(1–3):172–176. https://doi.org/10.1016/j.colsurfa.2010.10.013
35. Liu S, Tian JQ, Wang L, Zhang YW, Qin XY, Luo YL, Asiri AM, Al-Youbi AO, Sun XP (2012) Hydrothermal treatment of grass: a low-cost, green route to nitrogen-doped, carbon-rich, photoluminescent polymer nanodots as an effective fluorescent sensing platform for label-free detection of Cu(II) ions. Adv Mater 24(15):2037–2041. https://doi.org/10.1002/adma.201200164